Angular modulation of terahertz wavefront scattering based on all-silicon dielectric coded metasurface grating

SIQI SHI, KAI YANG*, XUFENG JING
Institute of Optoelectronic Technology, China Jiliang University, Hangzhou 310018, China

In order to simplify the design and fabrication difficulties, and to improve the efficiency of the transmission device, we designed an all-silicon monolayer coded metasurface grating. The single layer coded metasurface is composed of circular hole elements with different sizes. Based on the generalized Snell's law, we can know that the far-field scattering angle of the coded metasurface depends on the coding period. If we want to get different scattering angles, we need to design different coding periods. In general, the traditional coded metasurface sequence cannot realize the continuous control of the scattering angle. Here, by addition and subtraction of the coded sequence, a new coded metasurface sequence is obtained, and a new scattering angle is obtained. Through the addition and subtraction operations of coded metasurface sequences, we can obtain the flexible control of scattering angle without redesigning the coding unit.

(Received June 3, 2021; accepted April 8, 2022)

Keywords: Metasurface, Encoding sequence, Grating

1. Introduction

Electromagnetic metamaterials, also known as new artificial electromagnetic materials, are composite materials with periodic or quasi-periodic structure and specific electromagnetic properties, which are processed or synthesized by artificial means [1-10]. Compared with traditional materials, electromagnetic metamaterials use macroscopic size units instead of microscopic size units [11-20]. Recently, a two-dimensional artificial electromagnetic metasurface has attracted much attention. Metasurfaces can be considered as two-dimensional equivalents of metamaterials. Metasurface refers to a kind of artificial layered material whose thickness is smaller than wavelength. By designing geometric or electromagnetic parameters on a small scale, the characteristics of polarization, amplitude, phase, polarization mode and propagation mode of electromagnetic wave can be adjusted flexibly and effectively, so as to obtain controllable and specific electromagnetic characteristics. Metasurfaces have the advantages of negligible thickness, small physical space, simple preparation process, easy large-scale integration, and low loss. They are widely used in many fields, such as terahertz switching, vortex beam generation, electromagnetic cloaking, etc.[21-40].

Recently, with the rapid development of digital technology, it is difficult for the traditional analog metasurface to realize the digital control of electromagnetic information, and the encoding metasurfaces were proposed [41]. The coded metasurface uses digital states to represent electromagnetic parameters, which directly connects the digital technology at the information level with the metasurface technology at the physical level. The difference between the coded metasurface and the traditional metasurface is that the coded metasurface adopts a simpler and more effective digital coding method to regulate the electromagnetic wave. At present, most of the coded metasurface patterns focus on the design and preparation of encoding metasurfaces with metal materials, but the ohmic loss effect by metal materials can seriously affect the efficiency of devices [42-52]. Therefore, it is expected to use all dielectric materials with low loss to achieve high efficiency of coded metasurface. In addition, most transmission-coded metasurfaces are implemented with multilayer structures, which makes the design and fabrication more difficult.

In this paper, we design an all-silicon self-supported metasurface for regulating terahertz wave propagation using a circular hole all-silicon dielectric cell structure. A complete 2π transmission phase shift was obtained by changing the radius of the circular hole. Using the generalized Snell's law, the basic coding sequence structure realizes the anomalous transmission of a single beam at a certain angle. By using the addition and subtraction operations of digital coding unit structures based on coding metasurface sequences, the far field scattering angle can be controlled flexibly. There is no need to redesign the unit structure size of the coded metasurfaces. The theoretical calculation results are in good agreement with the numerical simulation results by using the finite integral method. These coded metasurfaces have a promising future in signal processing, digital communication, electromagnetic imaging and other fields.

2. Theory

2.1. Generalized Snell's theorem

A plane wave is incident onto the interface as shown in Fig. 1. Suppose there are two paths between points A and B, namely ADB and AEB, where the phase at D is ϕ and the phase at E is $\phi + d\phi$. According to Fermat's principle, the phase difference between ADB and AEB is 0. Similarly, the two paths between A and C are ADC and AEC respectively, and the phase difference is 0. So, we can get

$$(k_0 n_i \sin\theta_i\, dx + \phi + d\phi) - (k_0 n_t \sin\theta_t\, dx + \phi) = 0 \quad (1)$$

$$(k_0 n_i \sin\theta_i\, dx + \phi + d\phi) - (k_0 n_i \sin\theta_r\, dx + \phi) = 0 \quad (2)$$

where dx is the distance between two points, n_i and n_t are the refractive indices of the two media, θ_i , θ_r and θ_t represent the incident angle, reflection angle and refraction angle, respectively, wave vector is $K_0 = \frac{\lambda}{2\pi}$, λ is the wavelength of the incident wave. Define $d\phi/dx$ to represent the phase gradient along the x direction, then

$$n_t \sin\theta_t - n_i \sin\theta_i = \frac{\lambda}{2\pi}\left(\frac{d\phi}{dx}\right) \quad (3)$$

$$\sin\theta_r - \sin\theta_i = \frac{\lambda}{2\pi}\left(\frac{d\phi}{dx}\right) \quad (4)$$

That's the generalized Snell's law[46]. The traditional Snell's law is

$$\sin\theta_r - \sin\theta_i = 0 \quad (5)$$

When the incident angle is determined, the refraction angle is uniquely determined. But in the generalized Snell's law, when the incident angle is determined, you can change the refraction angle by changing $d\phi/dx$.

In this work,$n_i = n_t = 1$. The terahertz wave incidents vertically at the metasurface, so $\sin\theta_i = 0$, so the above generalized Snell's law can be simplified as

$$\sin\theta_t = \frac{\lambda}{2\pi}\left(\frac{d\phi}{dx}\right) \quad (6)$$

$$\sin\theta_r = \frac{\lambda}{2\pi}\left(\frac{d\phi}{dx}\right) \quad (7)$$

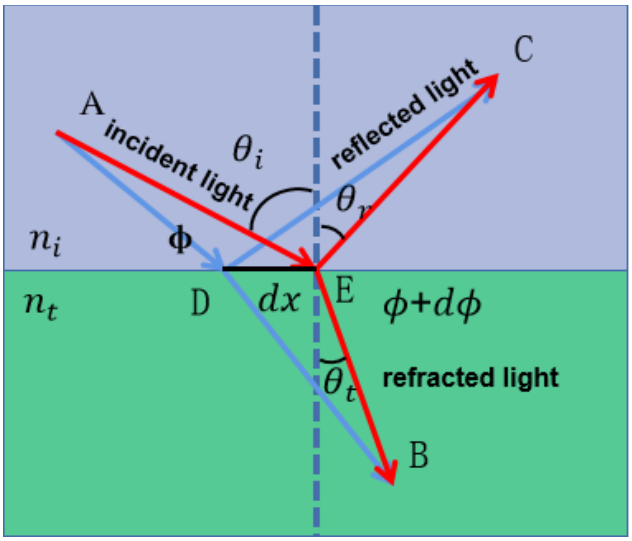

Fig. 1. Schematic diagram of generalized Snell's law (color online)

2.2. Diffraction grating theorem

An optical element that can periodically modulate the amplitude or phase of the incident light spatially, or both, is called a diffraction grating. Multi-slit diffraction is the result of interference of multiple single-slit diffraction beams with the same amplitude and the same optical path difference between adjacent beams. Suppose the complex amplitude of a single slit diffraction pattern at the most edge is

$$E(p) = E_0 \frac{\sin(\alpha)}{\alpha} \exp(i\delta_0) \quad (8)$$

For a diffracted plane with N slits, the complex amplitude is the result of the interference of N diffracted light, and the phase difference of the complex amplitude of adjacent diffracted light is $\delta = \frac{2\pi}{\lambda} d\sin\theta$. Therefore, its resultant complex amplitude is

$$\begin{aligned} E(p) &= E_0 \frac{\sin(\alpha)}{\alpha} \exp(i\delta_0)\{1 + \exp(i\delta) + \exp(i2\delta) + \cdots \\ &\quad + \exp[i(N-1)\delta]\} \\ &= E_0 \frac{\sin(\alpha)}{\alpha} \exp(i\delta_0) \frac{1 - \exp(iN\delta)}{1 - \exp(i\delta)} \\ &= E_0 \frac{\sin(\alpha)}{\alpha} \exp(i\delta_0) \frac{\sin(N\delta/2)}{\sin(\delta/2)} \exp[i(N-1)\delta/2] \end{aligned} \quad (9)$$

So the intensity is

$$I = I_0 \left(\frac{\sin\alpha}{\alpha}\right)^2 \left[\frac{\sin(N\delta/2)}{\sin(\delta/2)}\right]^2 \quad (10)$$

In fact, any aperture with a periodic arrangement, includes a two-dimensional arrangement or an aperture with a certain phase or amplitude modulation, has a similar conclusion, which is the result of the interaction between the diffraction of a single aperture and the interference of multiple beams.

The interference factor is a periodic function whose period $T = \delta_0 = 2\pi$.When

$$\delta = \frac{2\pi d\sin\theta}{\lambda} = 2m\pi \ (m = 0,\ \pm 1,\ \pm 2,\ \ldots) \quad (11)$$

or

$$d\sin\theta = m\lambda \ (m = 0,\ \pm 1,\ \pm 2,\ \ldots) \quad (12)$$

The interference factor has a maximum value N^2. These maxima are called principal maxima and m is their diffraction order. For the main maximum, their positions are only dependent on the grating constant d, and independent of the number of slits N[34-36]. The length of the structure corresponding to the unit structure designed in this paper in phase shift 2π is called as coding period Γ. Therefore, the above equation can also be written as

$$\sin\theta = \frac{\lambda}{\Gamma} \quad (13)$$

Suppose there are two metasurface grating sequences with different grating period, the diffraction angle of one grating is θ_1, and that of the other grating is θ_2.When we add or subtract the two metasurface grating sequences, the diffraction angle of the new grating sequence is θ'. Obviously θ' satisfy the formula as

$$\sin\theta' = \sin\theta_1 \pm \sin\theta_2 \quad (14)$$

The grating Eq.(12), which determines the position of the main maxima at each level, is now extended to the case of oblique incidence of the incident light. As shown in Fig. 2, when the incident light incident at an oblique angle of θ_i, the optical path difference between two adjacent beams should be added to the optical path difference introduced by the incident light, so the corresponding grating equation should be

$$d(\sin\theta_i \pm \sin\theta_t) = m\lambda \ (m = 0,\ \pm 1,\ \pm 2,\ \ldots) \quad (15)$$

The above equation shows that the diffraction angle θ_t is related to the wavelength of the incident light λ. The + or - in the formula corresponds to (a) and (b) in Fig. 2 respectively. When the incident angle and the refraction angle are on the same side of the normal line, it is positive; otherwise, it is negative.

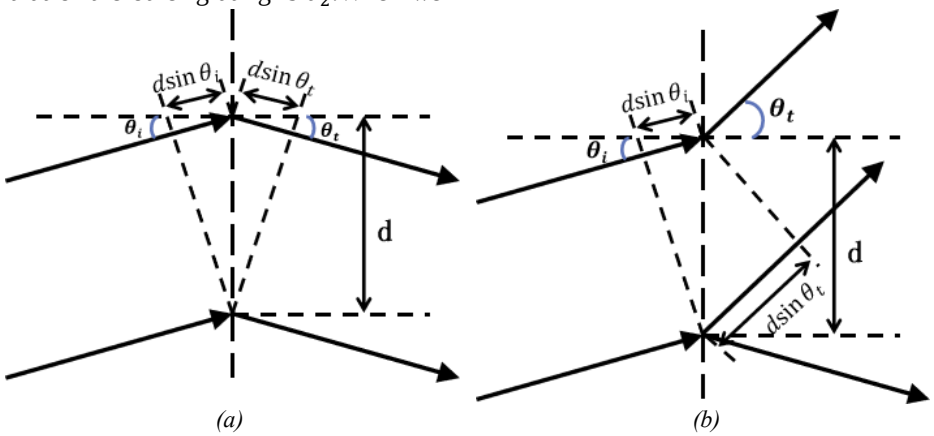

Fig. 2. Oblique incident diffraction grating

3. Metasurface grating design

We designed a round-hole all-silicon dielectric metasurface structure, as shown in Fig. 3. Among them, the silicon material with the relative permittivity ε of 11.9 and the magnetic permeability μ of 1 can obtain a higher transmission coefficient and thus improve the transmission efficiency. The finite integral method is often used to simulate unit structures [47]. In this simulation process, we obtain numerical results by finite integral method for strict vector electromagnetic theoretical calculation.

As can be seen from Fig. 3, the lattice constant P=200 μm, the thickness h=300 μm, the radius of the circular air hole is r, and the metasurface unit structure is designed by using the circular holes with different radii.

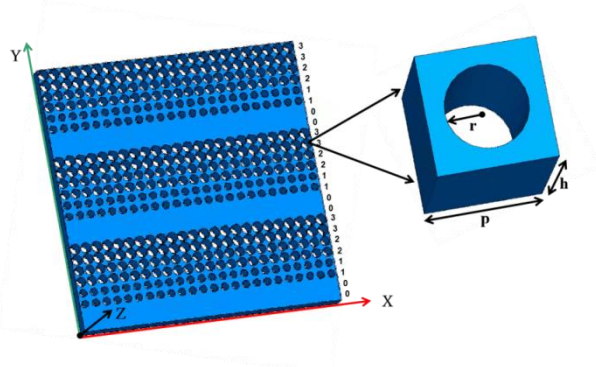

Fig. 3. Schematic diagram of all-silicon metasurface unit structure (color online)

The encoding metasurface consists of four coded cell structures. The finite integral method was used for simulation design. The excitation source was set as a plane wave, and the terahertz wave incident perpendicular to the

structure. The transmission efficiency and phase response within the frequency range of 0.2-0.8THz were obtained through the finite integral method of vector electromagnetic theory and parameter scanning optimization method, as shown in Fig. 4.

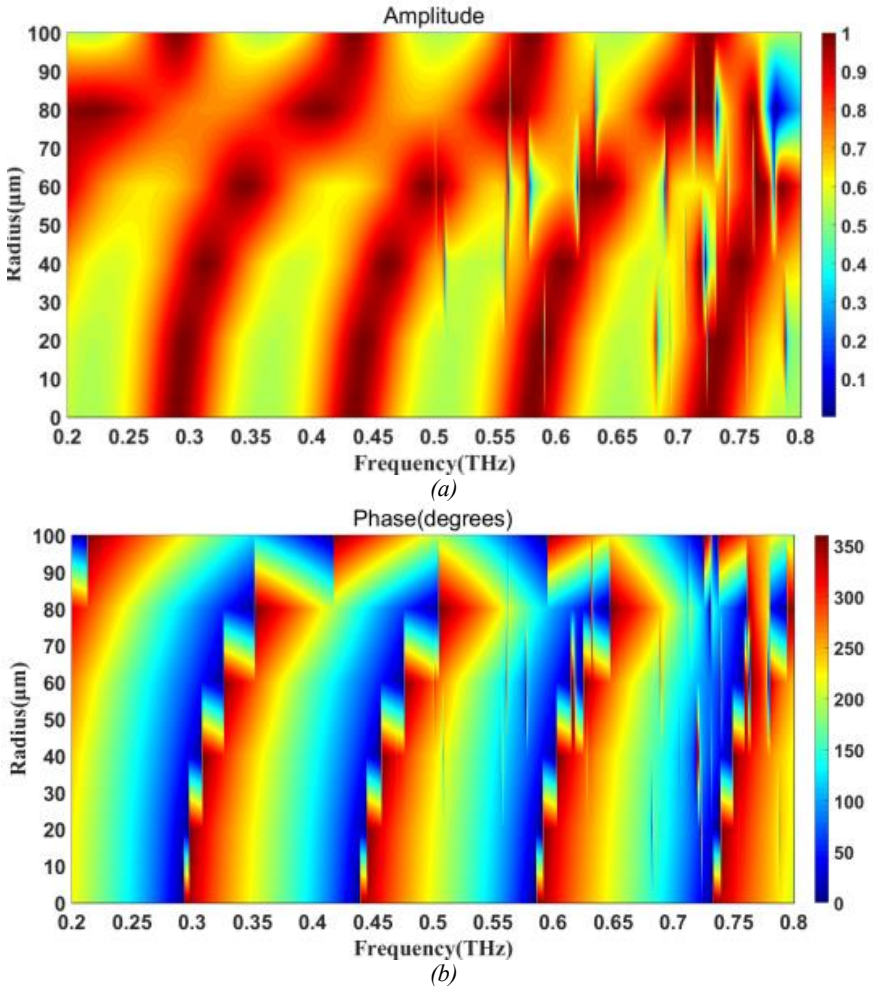

Fig. 4. The corresponding (a) analog transmission amplitude and (b) analog transmission phase at 0.2-0.8THz frequency (color online)

After optimization, the radius of the circular hole is r=0, r=69, r=86 and r=97 respectively, and the corresponding transmission phases are 0°, 90°, 180° and 270° four digital states respectively, as shown in Table 1. These four cells can be used to build a 2-bit coded metasurface, and these four unit structures can in turn be coded as "0", "1", "2", "3", respectively. Moreover, the transmission efficiency of the metasurface unit structures of the four units is all above 0.8, as shown in Fig. 5.

Table 1. The size of the circular hole, encoding mode, transmission amplitude and transmission phase of the metasurface unit structure

Code Block	Radius(μm)	Amplitude	Phase
00/0	0	0.9	30
01/1	75	0.8	130
10/2	86	0.9	207
11/3	97	0.9	298

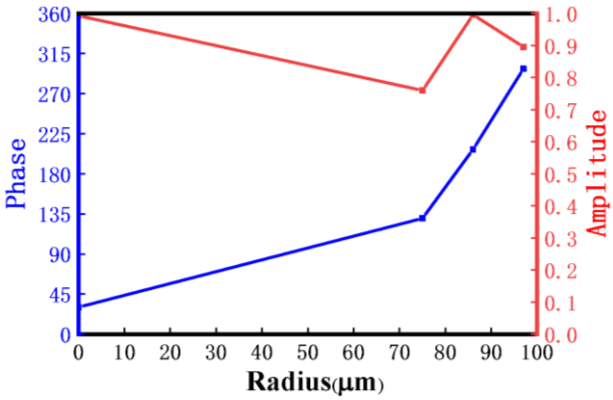

Fig. 5. The transmission amplitude and transmission phase of four cell structures with different circular hole sizes at $f=0.43THz$ (color online)

4. Far field scattering of metasurface grating

Next, a 2-bit coding unit is used to design the basic sequence of the encoding metasurface. Based on the optimized coding units obtained above, the metasurface of all-silicon dielectric designed by us is composed of basic sequences S1=00112233…, S2=000111222333… and S3=0000111122223333… composed of 24×24 coding units arranged periodically along the Y direction, as shown in Fig. 6(a). Each color represents a coding unit, with red, yellow, green and blue representing 0, 1, 2 and 3 coding units, respectively. Since the period of the coding unit is P=200μm, the periods of the basic coding sequences S1, S2 and S3 are Γ_{S1}=8P=1600 μm , Γ_{S2}=12P=2400 μm and Γ_{S3}=16P=3200μm, respectively. From formula $\lambda = C \times \nu$, we can get the incident wavelength λ =695.89 μm . According to the generalized Snell's theorem in Eq. (4), the theoretical transmission angles of the basic sequences S1, S2 and S3 coded metassurface can be calculated as 25.87°, 16.85° and 12.56°, respectively. As can be seen from the three-dimensional far field of Fig. 6(b), the transmission angles θ_1,θ_2 and θ_3 corresponding to sequences S1, S2 and S3 are 25°, 16° and 13°, respectively, which are in good agreement with the predicted theoretical values of 25.87°, 16.85° and 12.56°

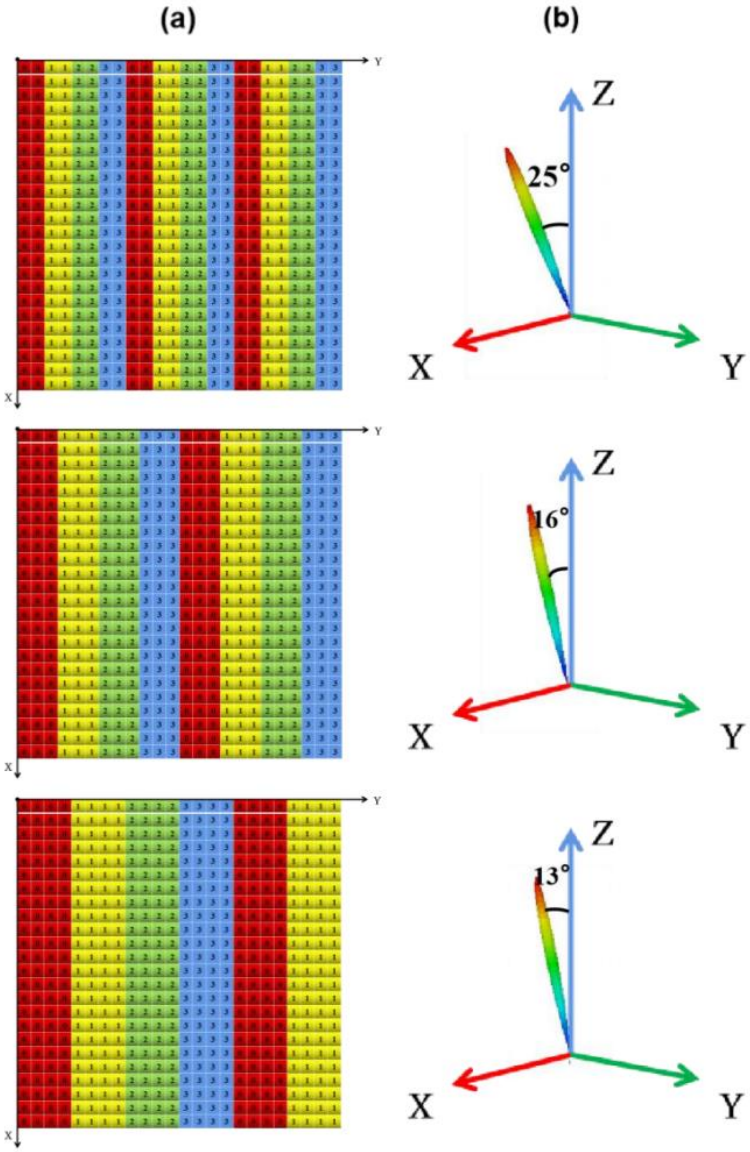

Fig. 6. (a) Color grid diagram of basic coding sequences S1, S2 and S3 and (b) Scattering pattern diagram (color online)

It is generally believed that continuous scanning angle can be achieved only by using continuous phase distribution. However, since the size of metasurface cells cannot be reduced indefinitely, continuous beam scanning cannot be achieved by using traditional coding methods. In order to control flexibly the transmission scattering angle of the encoded metasurface, we designed the new encoding sequences as S4=S1+S2=00123311230022301133012 2…,S5=S1+S3=0011330022331122001133 00… and S6=S2+S3=000122330111333011223000…with 24×24 encoding particles, then 1D encoding metasurface grating

can be formed by adding the above three basic coding sequences through adding numbers on each corresponding coding units. The structural schematics are shown in Fig. 7(a), (c) and (e) respectively. Due to the anisotropic structure of the one-dimensional grating, the transmission discrete angles of S4, S5 and S6 can be calculated by the grating equation in Eq.(14) as 46.57°, 40.83 and 30.49°, respectively. As shown in Fig. 7(b), (d) and (f), the transmission discrete angles obtained by the theoretical calculation of the designed one-dimensional grating metasurface is in good agreement with the simulation results.

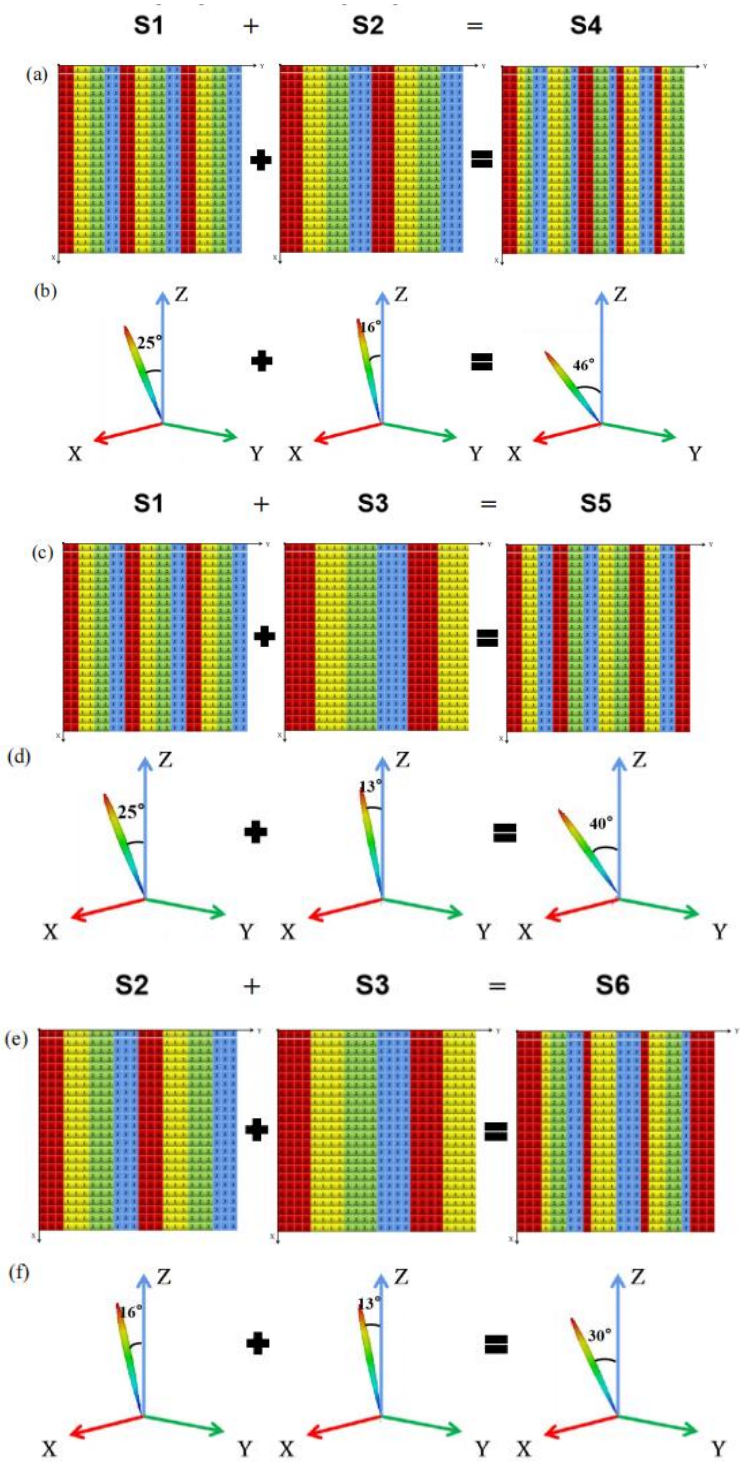

Fig. 7. (a) The basic coding sequences S1 and S2 are added to obtain S4.(b) The basic coding sequences S1 and S2 are added together to obtain the three-dimensional scattering pattern diagram of S4.(c) The basic coding sequences S1 and S3 are added to obtain S5.(d) The basic coding sequences S1 and S3 are added together to obtain the three-dimensional scattering pattern diagram of S5.(e)The basic coding sequences S2 and S3 are added to obtain S6.(f) The basic coding sequences S2 and S3 are added together to obtain the three-dimensional scattering pattern diagram of S6 (color online)

Similarly, the same theorem can be applied to subtraction operation on the basic encoding metasurface sequences. The negative sign of the basic coding sequence represents the opposite coding sequence. As shown in Fig. 8(a), (c) and (e), the subtraction operation is S7=S1-S2=330300001011112122223233…,S8=S1-S3=112222333300001111222233… and S9=S2-S3=111211221222222322332333…, respectively. According to the grating formula in Eq.(14), the transmitted discrete angles of S7, S8 and S9 can be calculated as 8.42°,12.64° and 4.15°, respectively. As shown in Fig. 8(b), (d) and (f), the transmission discrete angle obtained by the theoretical calculation of the designed one-dimensional grating metasurface is in good agreement with the simulation results.

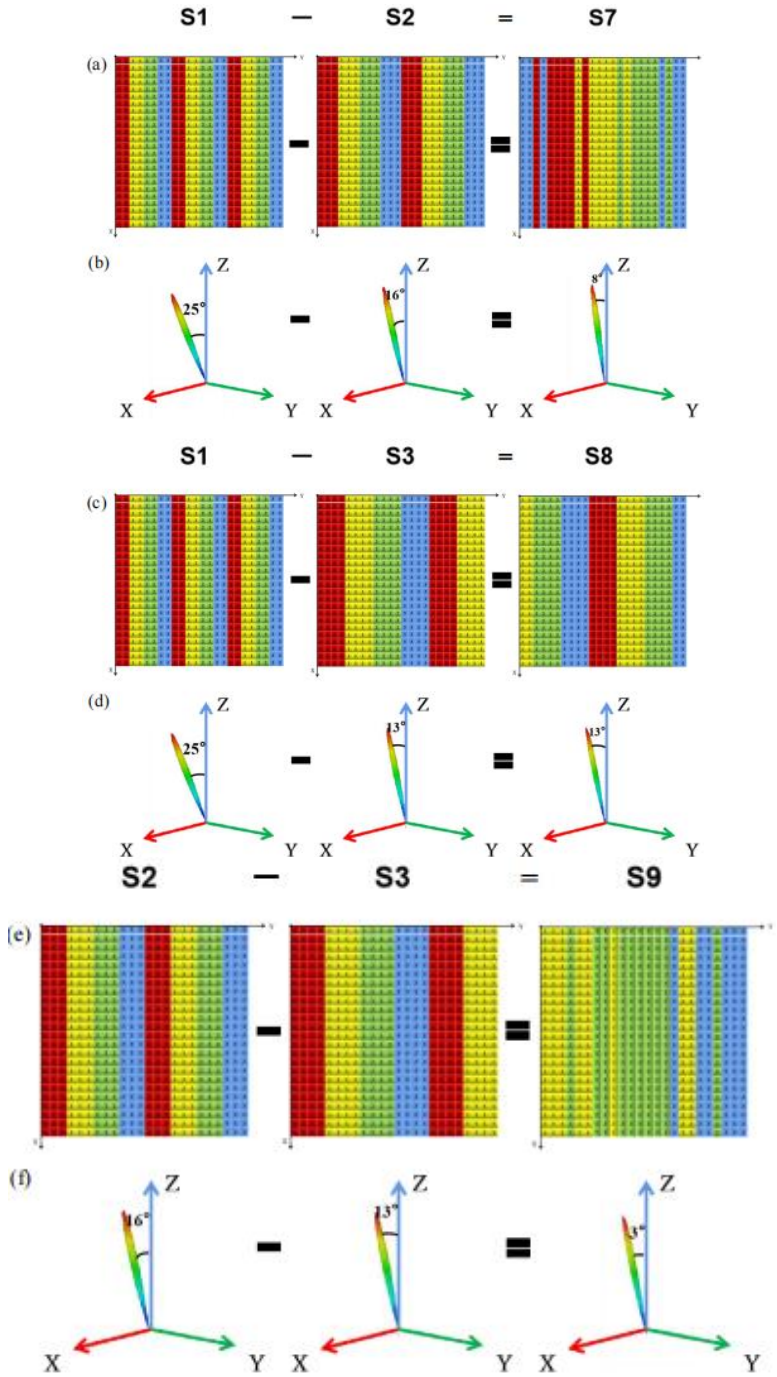

Fig. 8. (a)Subtract basic coding sequences S1 and S2 to obtain S7.(b)The basic coding sequences S1 and S2 are subtracted to obtain the three-dimensional scattering pattern diagram of S7.(c)Subtract basic coding sequences S1 and S3 to obtain S8.(d)The basic coding sequences S1 and S3 are subtracted to obtain the three-dimensional scattering pattern diagram of S8.(e)Subtract basic coding sequences S2 and S3 to obtain S9.(f)The basic coding sequences S2 and S3 are subtracted to obtain the three-dimensional scattering pattern diagram of S9 (color online)

Moreover, vortex beams can be generated by using the helical phase distributed on all-silicon dielectric metasurface. In order to generate vortex beam with topological charge number l=1, a phase plate of vortex beam with 24×24 element structure as shown in Fig. 9 is designed. The all-silicon dielectric metasurface is divided into four equal segments, the phase varies from 0 to 2π, and the phase difference of adjacent equal segments is $\pi/2$, which are arranged clockwise. Fig. 9(b) shows the far field amplitude distribution of the vortex beam. It can be seen that the center light intensity of the vortex beam is nearly 0. As can be seen from Fig. 9(c), the phase of vortex beam presents an obvious gradual change, that is, the wave front presents a spiral distribution.

Detailed preparation process of all dielectric metasurfaces in terahertz range refers to Ref. [53].The preparation processes include the base bonding, the conventional mask photolithography, and the Bosch deep reactive ion etching process.

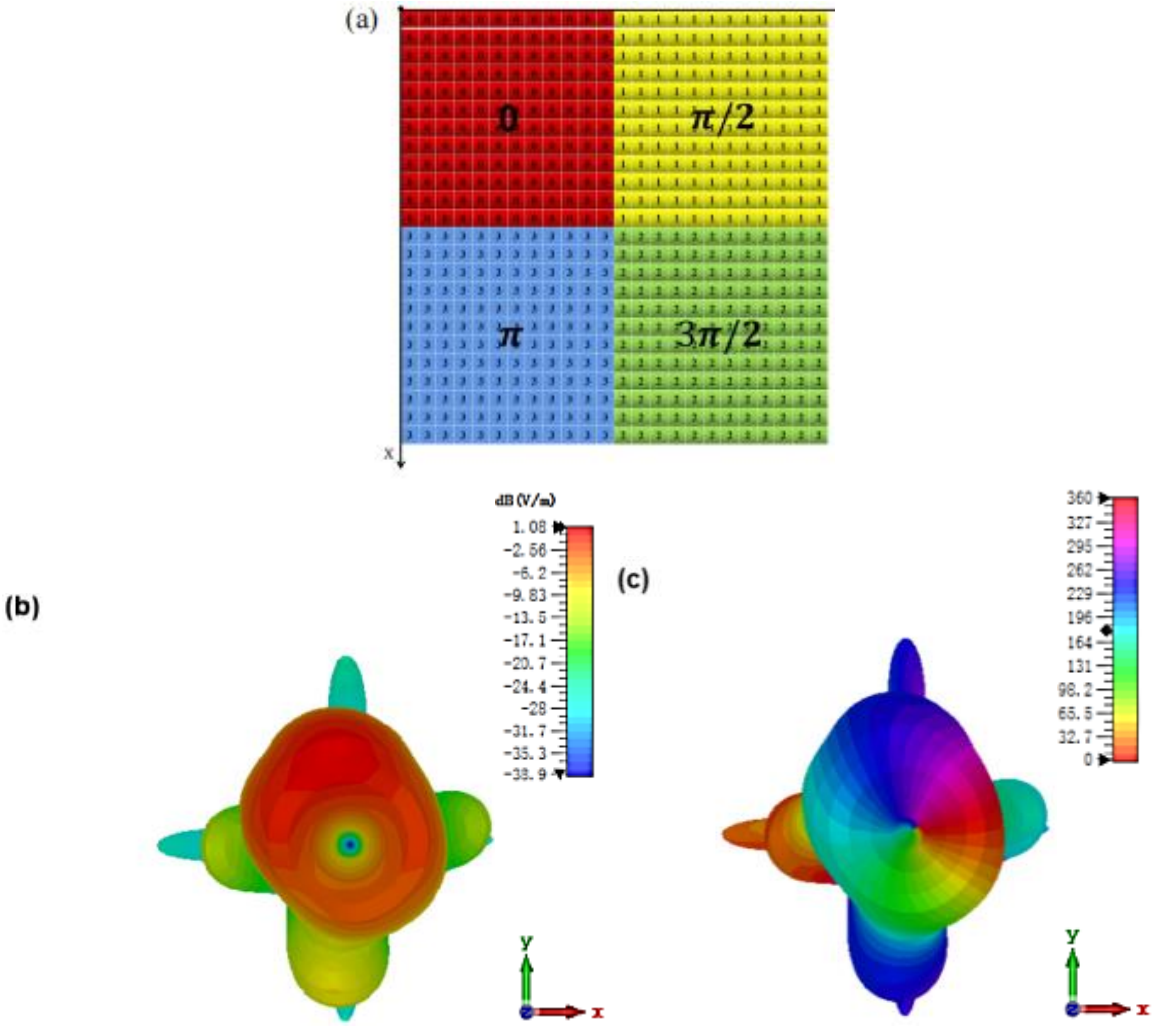

Fig. 9. (a) A schematic diagram of the hypersurface generated by the vortex beam when the topological charge number l=1; (b) a three-dimensional far-field scattering amplitude diagram of the vortex beam generated when the topological charge number l=1; (c) the three-dimensional far-field scattering phase diagram of the vortex beam generated when the topological charge l=1 (color online)

5. Conclusion

In summary, an all-silicon self-supported metasurface grating is designed with a circular hole type all-silicon dielectric unit structure. The complete transmission phase shift is obtained by changing the radius of the circular hole, and the terahertz wavefront scattering angle is controlled.

Based on the basic coding sequences and diffraction grating theory, several new coding sequences can be obtained by adding or subtracting these coding sequences. The far-field scattering angle can be flexibly controlled by adding and subtracting encoding metasurface sequences.

Acknowledgments

This work was supported by Natural Science Foundation of Zhejiang Province (Nos. LY20F050007 and LZ21A040003); National Natural Science Foundation of China (NSFC) (Nos. 61904169, 61904168, and 61875179).

References

[1] J. X. Huang, T. Fu, H. O. Li, Z. Y. Shou, X. Gao, Chinese Optics Letters **18**(1), 013102 (2020).
[2] L. Chen, D. G. Liao, X. Guo, J. Y. Zhao, Y. M. Zhu, S. L. Zhuang, Frontiers of Information Technology & Electronic Engineering **20**(5), 591 (2019).
[3] M. R. Akram, G. Ding, K. Chen, Y. Feng, W. Zhu, Advanced Materials **32**(12), 1907308 (2020).
[4] J. Zhang, X. Wei, I. D. Rukhlenko, H. T. Chen, W. Zhu, ACS Photonics **7**(1), 265 (2019).
[5] L. Li, Q. Yuan, R. Chen, X. J. Zou, W. B. Zang, T. Y. Li, G. G. Zheng, S. M. Wang, Z. L. Wang, S. N. Zhu, Chinese Optics Letters **18**(8), 082401 (2020).
[6] B. Fang, Z. Y. Cai, Y. D. Peng, C. X. Li, Z. Hong, X. F. Jing, Journal of Electromagnetic Waves and Applications **33**(11), 1375 (2019).
[7] B. Fang, B. Y. Li, Y. D. Peng, C. X. Li, Z. Hong, X. F. Jing, Microwave and Optical Technology Letters **61**(10), 2385 (2019).
[8] W. M. Wang, X. F. Jing, J. Y. Zhao, Y. Y. Li, Y. Tian, Optica Applicata **47**(2), 183 (2017).
[9] L. Jiang, B. Fang, Z. G. Yan, C. X. Li, J. P. Fu, H. Y. Gan, Z. Hong, X. F. Jing, Microwave and Optical Technology Letters **62**(6), 2405 (2020).
[10] J. Y. Xiao, R. W. Xiao, R. X. Zhang, Z. X. Shen, W. Hu, L. Wang, Y. Q. Lu, Chinese Optics Letters **18**(9), 092403 (2020).
[11] O. Olugh, Z. L. Li, B. S. Xie, High Power Laser Science and Engineering **8**(4), 04000e38 (2020).
[12] L. Xia, Y. Z. Hu, W. Y. Chen, X. G. Li, High Power Laser Science and Engineering **8**(3), 03000e28 (2020).
[13] J. Hornung, Y. Zobus, P. Boller, C. Brabetz, U. Eisenbarth, T. Kühl, Zs. Major, J. B. Ohland, M. Zepf, B. Zielbauer, V. Bagnoud, High Power Laser Science and Engineering **8**(2), 02000e24 (2020).
[14] F. Ding, Y. T. Chen, S. I. Bozhevolnyi, Photonics Research **8**(5), 707 (2020).
[15] X. Q. Zhang, Q. Xu, L. B. Xia, Y. F. Li, J. Q. Gu, Z. Tian, Advanced Photonics **2**(1), 014001 (2020).
[16] J. Zhang, H. Zhang, W. X. Yang, K. Chen, X. Z. Wei, Y. J. Feng, R. H. Jin, W. R. Zhu, Advanced Optical Materials **8**(19), 2000683 (2020).
[17] X. D. Bai, F. W. Kong, Y. T. Sun, G. F. Wang, J. Y. Qian, X. B. Li, A. J. Cao, C. He, X. L. Liang, R. H. Jin, W R. Zhu, Advanced Optical Materials **8**(17), 2000570 (2020).
[18] X. F. Jing, X. C. Gui, P. W. Zhou, Z. Hong, Journal of Lightwave Technology **36**(12), 2322 (2018).
[19] R. Xia, X. F. Jing, X. C. Gui, Y. Tian, Z. Hong, Optical Materials Express **7**(3), 977 (2017).
[20] M. R. Akram, M. Q. Mehmood, X. Bai, R. Jin, M. Premaratne, W. Zhu, Advanced Optical Materials **7**(11), 1801628 (2019).
[21] M. R. Akram, X. Bai, R. Jin, G. A. E. Vandenbosch, M. Premaratne, W. Zhu, IEEE Transactions on Antennas and Propagation **67**(7), 4650 (2019).
[22] J. Y. Zhao, X. F. Jing, W. M. Wang, Y. Tian, D. S. Zhu, G. H. Shi, Optics & Laser Technology **95**, 56 (2017).
[23] Y. Tian, X. F. Jing, H. Y. Gan, C. X. Li, Z. Hong, Frontiers of Physics **15**(6), 1 (2020).
[24] C. D. Zhou, Z. Mou, R. Bao, Z. Li, S. Y. Teng, Frontiers of Physics **16**, 33503 (2021).
[25] Y. Y. Fu, J. Q. Tao, A. L. Song, Y. W. Liu, Y. D. Xu, Front. Phys. **15**, 52502 (2020).
[26] J. P. Li, R. H. Jin, J. P. Geng, X. L. Liang, K. Wang, M. Premaratne, W. R. Zhu, IEEE Transactions on Antennas and Propagation **67**(4), 2442 (2018).
[27] X. Q. Lu, X. Y. Zeng, H. R. Lv, Y. S. Han, Z. Mou, C. X. Liu, S. Y. Wang, S. Y. Teng, Nanotechnology **31**(13), 135201 (2020).
[28] H. R. Lv, X. Q. Lu, Y. S. Han, Z. Mou, C. D. Zhou, S. Y. Wang, S. Y. Teng, New Journal of Physics **21**(12), 123047 (2019).
[29] H. R. Lv, X. Q. Lu, Y. S. Han, Z. Mou, S. Y. Teng, Optics letters **44**(10), 2518 (2019).
[30] H. Wang, L. X. Liu, C. D. Zhou, J. L. Xu, M. N. Zhang, S. Y. Teng, ORCID logo and Yangjian Cai, Nanophotonics **8**(2), 317 (2019).
[31] X. F. Jing, S. Z. Jin, Y. Tian, P. Liang, Q. M. Dong, L. Wang, Optics & Laser Technology **48**, 160 (2013).
[32] X. F. Jing, Y. N. Xu, H. Y. Gan, Y. W. He, Z. Hong, IEEE Access **7**, 144945 (2019).
[33] L. Jiang, B. Fang, Z. G. Yan, J. Fan, C. K. Qi, J. J. Liu, Y. W. He, C. X. Li, X. F. Jing, H. Y. Gan, Z. Hong, Optics & Laser Technology **123**, 105949 (2020).
[34] X. Y. He, Carbon **82**, 229 (2015).
[35] X. Y. He, X. Zhong, F. T. Lin, W. Z. Shi, Opt. Mater. Express **6**, 331 (2016).
[36] N. Mahmood, M. Q. Mehmood, F. A. Tahir, Scientific Reports **10**(1), 1 (2020).
[37] L. L. Lan, Y. M. Gao, X. C. Fan, M. Z. Li, Q. Hao, T. Qiu, Frontiers of Physics 16, 43300 (2021).
[38] P. Moitra, B. A. Slovick, W. Li, I. I. Kravchencko, D. P. Briggs, S. Krishnamurthy, J. Valentine, ACS Photonics **2**(6), 692 (2015).
[39] G. M. Akselrod, J. N. Huang, T. B. Hoang, P. T. Bowen, L. Su, D. R. Smith, M. H. Mikkelsen, Advanced Materials **27**(48), 8028 (2015).
[40] H. C. Chu, Q. Li, B. B. Liu, J. Luo, S. L. Sun, Z. H. Hang, L. Zhou, Y. Lai, Light: Science & Applications **7**(1), 1 (2018).
[41] T. J. Cui, M. Q. Qi, X. Wan, J. Zhao, Q. Cheng, Light: Science & Applications **3**(10), e218 (2014).
[42] K. Y. Liu, G. M. Wang, T. Cai, W. L. Guo, Y. Q. Zhuang, G. Liu, Chinese Physics B **27**(8), 084101 (2018).

[43] C. Pfeiffer, A. Grbic, Physical Review Letters **110**(19), 197401 (2013).
[44] F. Monticone, N. M. Estakhri, A. Alu, Physical Review Letters **110**(20), 203903 (2013).
[45] J. P. S. Wong, M. Selvanayagam, G. V. Eleftheriades, IEEE Transactions on Microwave Theory and Techniques, **63**(3), 913 (2015).
[46] V. R. Shrestha, B. Craig, J. J. Meng, J. Bullock, A. Javey, K. B. Crozier, Scientific Reports **10**(1), 1 (2020).
[47] L. D. Shao, M. L. Premaratne, W. R. Zhu, IEEE Access **7**, 45716 (2019).
[48] R. Dharmavarapu, S. H. Ng, F. Eftekhari, S. Juodkazis, S. Bhattacharya, International Society for Optics and Photonics **10456**, 104561W (2018).
[49] H. F. Zhang, X. Q. Zhang, Q. Xu, Q. Wang, Y. H. Xu, M. G. Wei, Y. F. Li, J. Q. Gu, Z. Tian, C. M. Ouyang, X. X. Zhang, C. Hu, J. G. Han, W. L. Zhang, Photonics Research **6**(1), 24 (2018).
[50] R. Y. Wu, C. B. Shi, S. Liu, W. Wu, T. J. Cui, Advanced Optical Materials **6**(5), 1701236 (2018).
[51] J. S. Li, C. Zhou, Optical Materials Express **11**(2), 310 (2021).
[52] M. Lawrence, D. R. Barton, J. Dixon, J. H. Song, J. Groep, M. L. Brongersma, J. A. Dionne, Nature Nanotechnology **15**(11), 956 (2020).
[53] Z. J. Ma, S. M. Hanham, P. Albella, B. H. Ng, H. T. Lu, Y. D. Gong, S. A. Maier, M. H. Hong, ACS Photon. **3**(6), 1010 (2016).

*Corresponding authors: yangkai@cjlu.edu.cn